PNAS RESEARCH ARTICLE | PHYSICS

Controlling laser-dressed resonance line shape using attosecond extreme-ultraviolet pulse with a spectral minimum

Yong Fu[a], Bincheng Wang[a], Kan Wang[a], Xiangyu Tang[a], Baochang Li[a], Zhiming Yin[a], Jiaxin Han[a], C. D. Lin[b], and Cheng Jin[a,c,1]

Edited by Stefano M. Cavaletto, Aarhus Universitet, Aarhus C, Denmark; received May 10, 2023; accepted December 1, 2023 by Editorial Board Member Shaul Mukamel

High-harmonic generation from a gas target exhibits sharp spectral features and rapid phase variation near the Cooper minimum. By applying spectral filtering, shaped isolated attosecond pulses can be generated where the pulse is split into two in the time domain. Using such shaped extreme-ultraviolet (XUV) pulses, we theoretically study attosecond transient absorption (ATA) spectra of helium $2s2p$ autoionizing state which is resonantly coupled to the $2s^2$ dark state by a time-delayed infrared laser. Our simulations show that the asymmetric $2s2p$ Fano line shape can be readily tuned into symmetric Lorentzian within the time delay of a few tens of attoseconds. Such efficient control is due to the destructive interference in the generation of the $2s2p$ state when it is excited by a strongly shaped XUV pulse. This is to be compared to prior experiments where tuning the line shape of a Fano resonance would take tens of femtoseconds. We also show that the predicted ATA spectral line shape can be observed experimentally after propagation in a gas medium. Our results suggest that strongly shaped attosecond XUV pulses offer the opportunity for controlling and probing fine features of narrow resonances on the few-ten attoseconds timescale.

attosecond transient absorption | doubly excited state | Fano resonance | Cooper minimum

Significance

Fano resonance is ubiquitous in nature, and the 2s2p resonance in helium atom is the most familiar one. By dressing a helium atom in an infrared laser field, its line shape can be modestly modified in standard XUV + IR experiments. Here, we show that dramatic change of the line shape (or Fano q-parameter) can occur within a few tens of attoseconds if an extremely shaped XUV pulse is used. Such pulses have been obtained via high-order harmonic generation with distinct Cooper minimum (like carbon dioxide). This work exemplifies extreme attosecond control of Fano resonance and electron dynamics.

Photoabsorption spectroscopy is an essential tool for studying the microscopic structure of matter. Using extreme ultraviolet (XUV) or soft X-rays, the absorption spectra in general consist of a smooth continuum imbedded with asymmetric Fano resonances (1). Fano resonance is a widespread wave-scattering phenomenon. It has been widely studied in atoms (2–4), molecules (5–8), nuclei (9, 10), solids (11), nanostructure (12), and acoustic systems. Since the asymmetric line shape is sensitive to the structure, as well as to the environment, the so-called topological Fano resonances have been found to have wide applications (13). With the emergence of attosecond XUV pules in the last two decades (14, 15), attosecond transient absorption (ATA) spectroscopy has been used to manipulate autoionization dynamics and to modify the asymmetric Fano line shape by coupling with infrared laser pulses (16–32). Taking the ATA spectra of the $2s2p$ doubly excited state of He as an example, an asymmetric Fano resonance would be observed in the absence of the coupling infrared laser. To achieve the most efficient control, it is best to choose a 540-nm laser that can couple efficiently with the $2s^2$ dark state. This scheme is shown in Fig. 1*A*, which is analogous to the level scheme used to achieve electromagnetically induced transparency (EIT). EIT is a coherent optical phenomenon that can render a medium transparent in a very narrow spectral range, where the corresponding optical refractive index would become very large, thus leading to slow light (33) or even stopped light (34). In this paper, we seek a powerful route for controlling Fano resonances from the symmetric Lorentzian to inverted Lorentzian, and to asymmetric ones with q-parameters varying from $+\infty$ to $-\infty$, or vice versa, on the attosecond time scale, achieved by using a shaped XUV pulse during the pumping process.

There are several ways to modify the line shape of a Fano resonance. One is to change the amplitude of the discrete state, the other is to change the phase of the continuum states, or change the phase between the two. Previously, Chu and Lin (23) proposed to use an IR laser to resonantly couple the discrete state with another autoionizing state to induce Rabi oscillation between them; thus, the amplitude of the discrete state can be modified, and thus the Fano line shape. By using an intense IR laser or XUV pulses from the free-electron laser (35–38), an additional phase of the discrete state is accumulated due to the induced energy shift. As an example, in ref. 39, the $2s2p$ Fano resonance was generated by a broadband attosecond pulsed XUV light. By coupling to a moderately intense 7-fs, 730-nm laser, it was observed that an asymmetric Fano line shape can be tuned to a symmetric Lorentzian one with $q \to \infty$, and vice versa. Here, the IR laser

Author affiliations: [a]Department of Applied Physics, Nanjing University of Science and Technology, Nanjing, Jiangsu 210094, China; [b]Department of Physics, James R. Macdonald Laboratory, Kansas State University, Manhattan, KS 66506; and [c]Ministry of Industry and Information Technology Key Laboratory of Semiconductor Microstructure and Quantum Sensing, Nanjing University of Science and Technology, Nanjing, Jiangsu 210094, China

Author contributions: C.D.L. and C.J. designed research; Y.F. and C.J. performed research; Y.F., B.W., K.W., X.T., B.L., Z.Y., J.H., C.D.L., and C.J. analyzed data; and Y.F., C.D.L., and C.J. wrote the paper.

The authors declare no competing interest.

This article is a PNAS Direct Submission. S.M.C. is a guest editor invited by the Editorial Board.

[1]To whom correspondence may be addressed. Email: cjin@njust.edu.cn.

This article contains supporting information online at https://www.pnas.org/lookup/suppl/doi:10.1073/pnas.2307836121/-/DCSupplemental.

Published January 3, 2024.

induces an energy shift of the bound state. By changing the laser intensity and duration, the phase between the bound and the continuum states is modified resulting in the change of the Fano q parameter. However, a significant change in the spectral line shape (or q parameter) has not been achieved by either directly changing the amplitude of the discrete state or by modifying the XUV pulse to excite the resonance states. Here, we show that dramatic control of the line shape can be achieved using shaped XUV pulses obtained from high-harmonic spectra generated near the Cooper minimum, where both the amplitude and phase undergo extreme variation over a very narrow energy range (sub-eV).

It has been established that high-harmonic generation (HHG) spectra mimic the photo-recombination (PR) cross-sections (40). Since PR amplitude varies rapidly and its phase changes greatly by near π if the atomic target has a narrow Cooper minimum, such rapid change also would occur in the amplitude and phase of the HHG spectra. By spectral filtering, the temporal XUV pulse around the Cooper minimum would be severely shaped, as shown in the case of the Ar atom (41). Similar spectral minima, but even much sharper, are present in the molecular HHG spectra when molecules are transiently aligned (42–44). Recently, Jin et al. (45, 46) demonstrated that the minimum structure in the HHG of aligned CO_2 molecules can be controlled by fine-tuning molecular alignment and thus the temporal shape of the synthesized XUV pulses can be readily shaped. For CO_2 molecules, the minimum occurs near 60 eV (42, 47), which is close to the energy of the helium $2s2p$ state. We show here that the asymmetric Fano profile can be dramatically tuned within attoseconds timescale using these exquisitely shaped XUV pulses.

In this article, we utilize a pump–probe scheme to investigate the modification of the Fano resonance profile in which the pump is an exquisitely shaped XUV pulse and the probe is an IR laser of a wavelength of 540 nm which resonantly couples the two autoionizing $2s2p$ and $2s^2$ states, as depicted in Fig. 1*A*. In the time domain, the electric field amplitude of a shaped XUV pulse has a sharp minimum at the center as if it has split into two pulses, which is in strong contrast to a typical Gaussian pulse; see Fig. 1*B*. Note that the structure of a double XUV pulse as shown in Fig. 1*B* has been demonstrated in an attosecond pulse train experimentally (41). In Fig. 1*C*, this shaped XUV pulse in the spectral domain has a minimum of 60.15 eV. More importantly, the spectral phase change by π within about 0.05 eV. To obtain the attosecond transient absorption (ATA) spectrum, we solve the time-dependent Schrödinger equation (TDSE) of helium atoms using a multi-level model (*SI Appendix*, section 1).

Results

The single-atom ATA spectra as a function of time delay between XUV and IR fields are plotted in Fig. 1 *D* and *E*, for the Gaussian and the shaped XUV pulse, respectively. For the Gaussian one, the spectra in Fig. 1*D* are consistent with those studied in refs. 23 and 48. For time delays where the two pulses overlap, as shown in Fig. 1*G*, the resonance profiles change shape only modestly with time delay. On the other hand, for the shaped XUV pulse, as shown in Fig. 1*E*, the time-delay dependent spectra are quite different. Here, we focus on how the line shape of the resonance varies in small increments of time delays in Fig. 1 *H* and *I*. First, in Fig. 1*H*, we note that at a time delay of −0.45 fs, the line shape appears as a deep window resonance with $q = 0$. With a small increment of 0.09 fs later at −0.36 fs, the line shape changes quickly to an asymmetric negative-q Fano resonance. For another increase of only 0.02 fs (or 20 as) at a time delay of −0.34 fs, the line shape changes drastically to an even larger value of negative q. At a time delay of 0.0 fs, the line shape changes quickly to a narrow Lorentzian shape. Proceeding to longer time delays, as shown in Fig. 1*I*, similar rapid changes of line shapes can be seen in reverse order for time delays of 0.0, 0.24, 0.28 fs, and finally, at a time delay of 0.45 fs, where the line shape returns to the same one as at a time delay of −0.45 fs. This shows that the Fano line

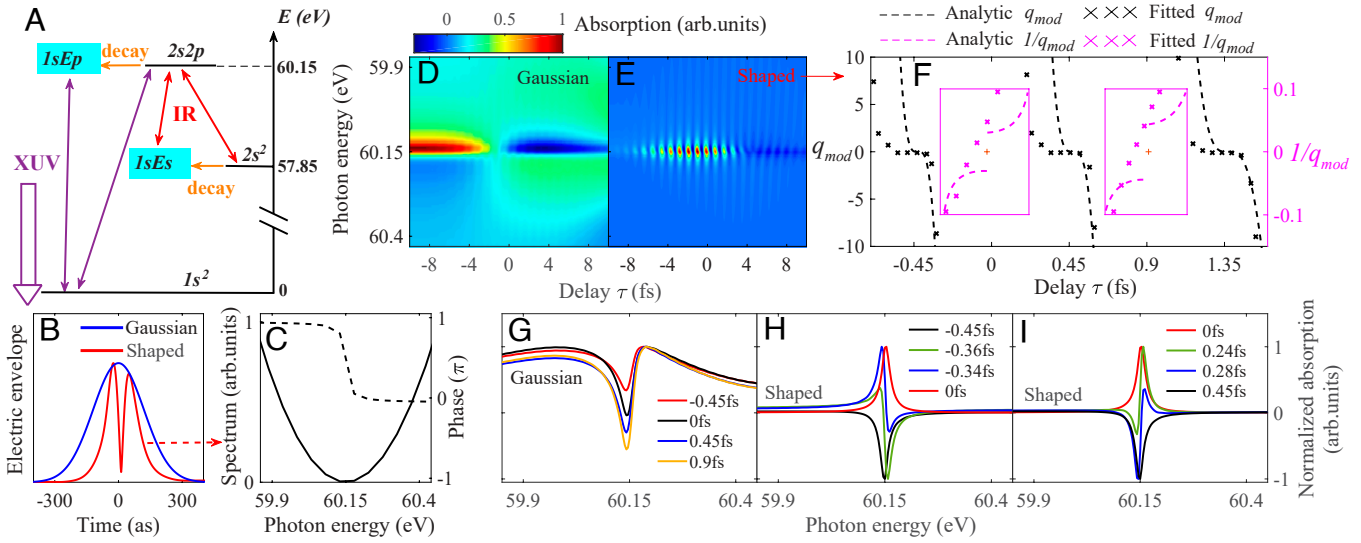

Fig. 1. (*A*) Schematic of a three-level model of a helium atom, including the ground state $1s^2$, autoionizing states $2s2p$ and $2s^2$, and continuum states $1sEp$ and $1sEs$, where E is the energy of the continuum electron. In this model, the XUV pulse pumps the system from $1s^2$ to $2s2p$ and $1sEp$ states, and the IR laser couples $2s2p$ and $1sEs$ states and also $2s2p$ and $2s^2$ states. Through configuration interaction, the system decays from $2s2p$ to $1sEp$ state and from $2s^2$ to $1sEs$ state. (*B*) Electric envelopes of a Gaussian (blue) and a shaped (red) XUV pulses. (*C*) Spectral distributions of amplitude (solid line) and phase (dashed line) of a shaped XUV pulse taken from ref. 45. Single-atom ATA spectra from a Gaussian (*D*) and a shaped XUV (*E*) pulse. Parameters of the XUV pulse: duration is ~ 200 as, peak intensity is 10^{10} W/cm^2, and central frequency is 60.15 eV. Parameters of the dressed IR laser: pulse duration is 9 fs, carrier frequency is 2.3 eV (period is 1.8 fs), peak intensity is 2×10^{12} W/cm^2, and carrier-envelope phase is 0. A positive time delay means the XUV pulse is ahead of the IR laser. (*F*) Analytic (dashed line) and fitted (dot) q parameters for the ATA spectra using the shaped XUV pulse. (*G–I*) The absorption spectral lines (normalized) at selected time delays; see text.

shape changes repetitively over 0.9 fs, which is half of the optical period of the driving 540-nm laser. These results demonstrate the dramatic efficient control of the resonance line shape when a shaped XUV pulse is used for studying ATA spectra for a narrow field-free resonance. We further fit the calculated line shape to obtain the q-parameter. In Fig. 1*F*, we plot how q changes with time delay. In the region where $|q|$ becomes larger than 10, we plot the values of $1/q$. For the present example, q changes rapidly within a few tens of attoseconds is clearly seen. In Fig. 1*F*, we also show the q values calculated using the analytical formula in Eq. **2**. Both the fitted and analytical results show that q varies from $+\infty$ to 0 and then from 0 to $-\infty$ during half of the optical period of the IR laser. We point out that the results shown above for absorption spectra are expected to appear in photoelectron spectra (*SI Appendix*, Figs. S4–S7), but photoelectron spectra are much more difficult to observe experimentally due to challenges in high-resolution electron spectra.

Discussion

To explain the difference in the change of ATA spectra for the Gaussian and the shaped XUV pulses, we examine the growth of populations of the two autoionizing states $2s^2$ and $2s2p$ for the case where the time delay is zero. For the Gaussian pulse, we see in Fig. 2*A* that the population builds up monotonically with time for both states. For $2s2p$, the time-dependent buildup is the same even if its coupling with the continuum states is turned off (without configuration interaction) or the IR laser is absent. For the shaped XUV pulse, both states build up gradually up to $t = 0$. In the second half for $t > 0$, the $2s2p$ population drops with time, but the $2s^2$ population stays constant; see Fig. 2*B*. Interestingly, the population of the dark state $2s^2$ is higher than the bright state $2s2p$ at the end of the XUV pulse. This figure also shows that coupling with continuum states or the absence of IR laser does not affect the buildup of $2s2p$. This is not surprising since the field-free lifetime for $2s2p$ is about 17 fs while the pulse duration of the shaped XUV is only about 200 as.

We next show the population of $2s2p$ and $2s^2$ at the end of the XUV pulse versus the time delay in Fig. 2 *C* and *D*. For the Gaussian XUV, the population of the dark state $2s^2$ is very small and can be neglected. But for the shaped XUV pulse, the population of the $2s^2$ dark state is larger than the bright state $2s2p$. Both show rapid half-IR-optical-cycle oscillations with time delay. Fig. 2*D* shows population inversion occurs when the XUV pulse is a shaped one. In *SI Appendix*, section 8, we examine how this happens in detail. In the time domain where the XUV pulse overlaps with the IR laser, the XUV pulse excites the $2s2p$ state, but the IR laser couples the $2s2p$ state to the $2s^2$ state. Since a shaped XUV pulse in the time domain is a double-pulse where the second pulse interferes destructively with the first one such that the $2s2p$ population declines with time while the $2s^2$ population stays constant; see Fig. 2*B*. After the XUV pulse ends, the IR laser drives the electron between the $2s2p$ and $2s^2$ states. Using the IR intensity in the example, the Rabi frequency was calculated to be 9.3 fs longer than 1.8 fs, which is the optical period of the 540-nm laser.

In *SI Appendix*, section 8, we show that the population of the $2s^2$ state grows with IR intensity and population inversion can occur only when IR intensity is sufficiently high; see *SI Appendix*, Fig. S9. The dependence of population inversion on the time delay can be seen in Fig. 2*E* and *SI Appendix*, Fig. S9. For completeness, we also show the populations of $2s2p$ and $2s^2$

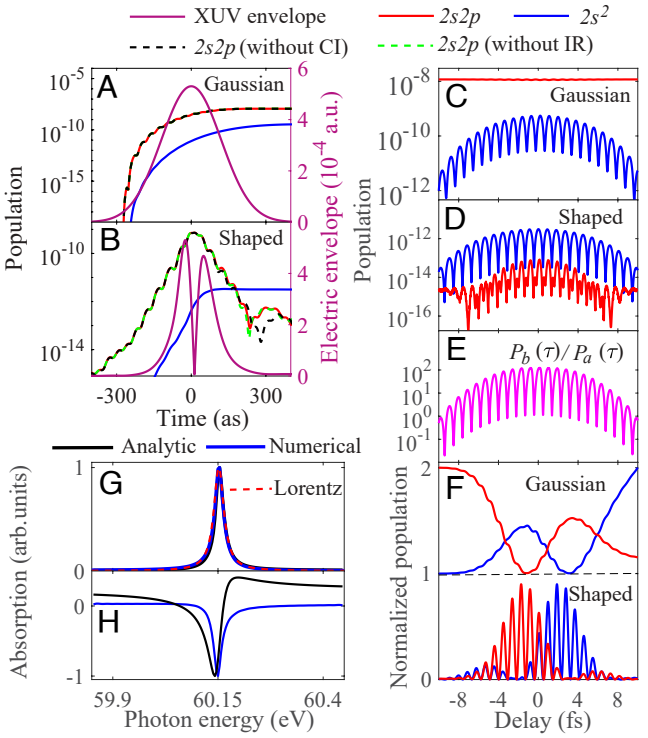

Fig. 2. (*A* and *B*) Populations of $2s2p$ (red solid lines) and $2s^2$ (blue solid lines) states at a time delay of 0 fs between the XUV pulse and the IR laser. In addition, the populations of $2s2p$ state without the IR laser (dashed green lines) and without the autoionizing configuration interaction (CI) (dashed black lines) are shown. Electric field envelopes of Gaussian and shaped XUV pulses are given (purple solid lines). Note that the population of $2s2p$ by shaped XUV pulse undergoes a sharp drop in the second half of the pumping process. (*C* and *D*) Populations of $2s2p$ and $2s^2$ states at the end of the XUV pulse as a function of time delay. (*E*) The ratio of $2s^2$ and $2s2p$ populations from (*D*). (*F*) Normalized populations of $2s2p$ and $2s^2$ states (plotted in linear scale) after complete shutdown of external fields as a function of time delay. Results for Gaussian pulse are moved up by one in arbitrary units. Comparison of absorption spectral lines using the shaped XUV pulse at time delays of 0 fs (*G*) and 0.45 fs (*H*) obtained by numerical solutions of TDSE and analytic solutions in Eq. **1**. The dashed line in (*G*) is the fitted Lorentz curve.

states at $t = 54$ fs where both the XUV pulse and the IR laser are long gone, versus the time delay in Fig. 2*F*. From the population dynamics, the absorption spectra versus the time delay can be calculated. Fig. 2*G* shows that the line shape of the $2s2p$ state at a time delay equal to zero is a Lorentzian, but becomes an inverted Lorentzian (or a window resonance) when the time delay is at 0.45 fs.

To understand the origin of the peculiar absorption spectra by the shaped pulse, using a few "reasonable" approximations, we can derive the single-atom absorption spectrum $S(\omega)$ (*SI Appendix*, section 6)

$$S(\omega) \propto \left[\cos\frac{A_L}{2}\frac{(q+\varepsilon)^2}{1+\varepsilon^2} + \left(1-\cos\frac{A_L}{2}\right)\right] + \sqrt{\frac{p_b(\tau)}{p_a(\tau)}}\sin\frac{A_L}{2}\mathrm{Re}\left[\frac{E_X(\omega_a)}{E_X(\omega)}\frac{(q+i)^2}{1+i\varepsilon}\right]. \quad [1]$$

This equation works for a general XUV pulse. Here, $\varepsilon = 2(\omega-\omega_a)/\Gamma$ is the reduced energy measured from the resonance, and ω_a and Γ are the resonance energy and width, respectively. The $p_a(\tau)$ and $p_b(\tau)$ are the populations of $2s2p$ and $2s^2$ states at the end of the XUV pulse for the time delay

τ, respectively. For the shaped XUV, the ratio $p_b(\tau)/p_a(\tau)$ is given in Fig. 2*E*. The complex $E_X(\omega)$ includes the spectral amplitude and phase of the XUV pulse. The pulse area of the IR laser is denoted by A_L (*SI Appendix*, section 2 and Fig. S3). In Eq. **1**, the second term on the right-hand side is dominant when $p_b(\tau)$ is much larger than $p_a(\tau)$. Since $p_b(\tau)$ is mostly dependent on the instantaneous intensity of the IR laser, the absorption spectra exhibit pronounced modulations with half optical period of the IR laser. Such modulations do not depend much on the pulse duration of the IR laser so long as the pulse area remains large when the intensity and duration are properly chosen.

We also give the modulated Fano q parameter when the probe IR laser is applied (*SI Appendix*, section 5)

$$q_{mod} = \left[\cos\frac{A_L}{2} - \sqrt{\frac{p_b(\tau)}{p_a(\tau)}}\frac{\sin(2\omega_L\tau)}{|\sin(2\omega_L\tau)|}\sin\frac{A_L}{2}\right]q. \qquad [2]$$

Here, ω_L is the frequency of IR pulse. When time delay is 0 fs, $p_b(\tau)$ is much larger than $p_a(\tau)$ as shown in Fig. 2*D*, thus $q_{mod} \to \infty$ by considering that $A_L = 1.45\pi$. Thus, a symmetric Lorentzian line shape arises in Figs. 1*H* and 2*G*. Moreover, as long as $p_b(\tau)$ is much larger than $p_a(\tau)$ and $\sin(A_L/2) \neq 0$, the Lorentzian line shape is obtained.

We further interpret why the population of the discrete state is dramatically decreased with the shaped XUV pulse. We first separate the whole temporal XUV pulse into two sub-pulses and transform each individual into the frequency domain. The phase difference between these two sub-pulses is found to be π at the spectral minimum ω_a (*SI Appendix*, section 4). Next, we concentrate on the XUV spectrum in the vicinity of ω_a and approximate each as monochromatic waves. Then, we employ a two-level model as sketched in Fig. 3*A*, in which the energy difference is exactly equal to the photon energy at the XUV minimum, i.e., $\omega_a = E_a - E_g$ (in atomic units). The time-dependent wave function is written as $|\psi(t)\rangle = c_g(t)\,e^{-iE_g t}|g\rangle + c_a(t)\,e^{-iE_a t}|a\rangle$ with ground state $|g\rangle$ and excited state $|a\rangle$. The wave function is then solved before and after t_0. Here, t_0 corresponds to the minimum position in the temporal envelope of the shaped XUV pulse, in which the peak amplitudes are A_1 and A_2, respectively. The time-dependent coefficient is (*SI Appendix*, section 7)

$$c_a(t) = \begin{cases} \frac{1}{2}D_{ag}A_1\left(it + \frac{1}{2\omega_a}e^{2i\omega_a t} - \frac{1}{2\omega_a}\right), 0 \le t \le t_0 \\ -\frac{1}{2}D_{ag}A_2\left[i(t-t_0) + \frac{1}{2\omega_a}\left(e^{2i\omega_a t} - e^{2i\omega_a t_0}\right)\right] \\ \qquad + c_a(t_0), t > t_0. \end{cases} \qquad [3]$$

Here, D_{ag} is the transition matrix element between states $|g\rangle$ and $|a\rangle$.

The population of the excited discrete state as a function of time (black line) obtained from the analytical solution in Eq. **3** is plotted in Fig. 3 *B* and *C*. To check the accuracy of Eq. **3**, we also solve the coupled equations of the two-level system exactly. A shaped XUV pulse can be composed of two regular Gaussian pulses by properly adjusting the time delay and their relative carrier-envelope phase such that the position and depth of the shaped XUV pulse are reproduced. The numerically obtained populations (red lines) are plotted in Fig. 3 *B* and *C*. For both shaped XUV pulses, the numerical and analytical solutions agree quite well and both show the decrease of the population in the second half of the pulse, more so for $A_2 = A_1$ than for $A_2 = 0.6A_1$. Therefore, when using an XUV pulse with a spectral minimum to pump the atomic system, the decrease of the population of discrete states in the Fano resonance is quite general. By adjusting A_1 and A_2, which can be carried out by adjusting the depth and position of the spectral minimum in the shaped XUV pulse, the ATA spectrum can be controlled. The shaped XUV pulse in turn can be controlled by manipulating the minimum in the HHG spectra which has been demonstrated recently by varying the degree of alignment of CO_2 molecules (45, 46).

For an experimental demonstration of the predicted features of a Fano resonance, we need to address the propagation of the absorption spectra in a macroscopic gas medium. The ATA spectrum after propagation in a gas medium is defined by the optical density (OD): $OD(\omega,\tau) = -\log[I(\omega,\tau)/I_0(\omega)]$, where $I(\omega,\tau)$ and $I_0(\omega)$ are XUV spectra at the exit and the entrance of the gas medium, respectively. One-dimensional Maxwell's wave equation in the moving frame is solved (*SI Appendix*, section 1). Comparing to single-atom absorption spectra in Fig. 1*E*, the OD of the shaped XUV spectra after propagation of 0.5 mm at a gas pressure of 25 Torr is shown in Fig. 4*A*. One can see the strong difference as the OD changes from absorption to emission (49) for time delays from −8 fs to 2 fs in a very short propagation distance. For a lower pressure of 5 Torr and the propagation distance of 0.1 mm, the OD becomes similar to the single-atom ATA spectrum, i.e., the absorption shows oscillation of half period of the IR laser; see Fig. 4*B*. In addition, both Lorentzian and inverted Lorentzian line shapes appear with little suffering from the propagation in a gas medium; see Fig. 4*D*. Furthermore, in Fig. 4*D*, the maximum OD (without normalization) for Lorentzian is 0.56, meaning that 73% of the XUV intensity is absorbed, while the minimum OD for the inverted Lorentzian line shape is −0.1, meaning that 26% of the XUV intensity is emitted. Thus, absorption and emission can be effectively observed experimentally.

Finally, we address the possible requirements for experimentalists to observe our simulated results. Our simulation assumes that the minimum of the shaped pulse is at 60.15 eV. The first concern is how far away the predicted minimum in the XUV pulse can be tolerated if our predicted attosecond control on the Fano line

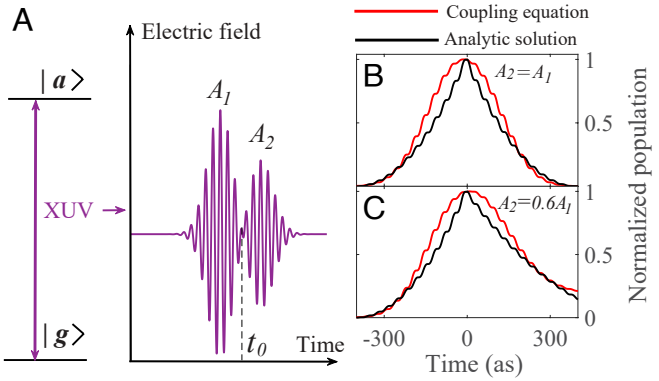

Fig. 3. (*A*) Sketch of a two-level model with the ground state $|g\rangle$ and an excited state $|a\rangle$ (*Left*), and the temporal profile of a shaped XUV pulse with two peak amplitudes, A_1 and A_2 (*Right*). (*B*) Population (normalized) of the excited state vs time when $A_2 = A_1$. (*C*) Same as (*B*) but for $A_2 = 0.6A_1$. Results obtained by numerical solutions of coupled equations (red lines) are compared to analytic solutions of Eq. **3** (black lines).

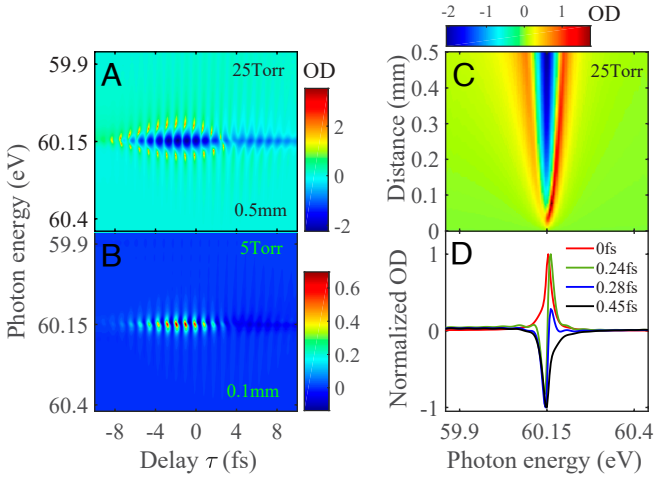

Fig. 4. (*A*) Optical density (OD) after propagation in a 0.5-mm long gas with a pressure of 25 Torr by a shaped XUV pulse. (*B*) Macroscopic OD in a gas with a length of 0.1 mm and pressure of 5 Torr. (*C*) Macroscopic OD as a function of propagation distance at 25 Torr when the time delay is fixed at 0 fs. (*D*) OD lines in (*B*) for selected time delays.

shape can be seen in the ATA spectra. In Fig. 5, we show the ATA spectra when the position of the XUV minimum is shifted by 0.3, 0.9, and 1.6 eV, respectively. The top row of Fig. 5 shows that for a deviation less than 0.3 eV, the main features of the change of the line shape, as well as the half-cycle modulations can all be seen clearly. With larger shifts of 0.9 and 1.6 eV, the major features of the line shape can also be seen, except that they are not as "sharp." The second concern is about the strength of the double-peak pulse which is from the HHG around the Cooper minimum. We have analyzed the experimental HHG data of Rupenyan et al. (44) for CO_2 molecules that are not aligned and that are aligned. Only the latter has the deep minimum. We conclude that the pulse energy of the shaped pulse is about eight times weaker than the typical Gaussian XUV pulses. We comment that such yields can be further increased by optimizing the phase matching (50, 51) and by the development of high-power, high-repetition-rate lasers shortly (52, 53). The third possible issue is how accurately the time delay is required. Our simulations in Figs. 1 and 5 show that dozens of attoseconds resolution is required to see the rapid change of absorption line shape. Since the shaped XUV pulses proposed in this work still have not been examined by experimentalists so far, that might be the first priority at this time.

Summary and Outlook

We demonstrated that a shaped XUV pulse can be used to significantly modify the asymmetric Fano line shapes under the XUV + IR scheme simply by changing the time delay between the two pulses, with dramatic shape change within tens to hundreds of attoseconds. Such sensitivity requires that the shaped XUV pulse have near phase change of π and deep minimum in the spectral domain, which in turn means that in the time domain, the XUV pulse is split into two nearly identical sub-pulses. It has been shown that such pulses can be obtained from high harmonics generated from CO_2 and other molecules where the so-called Cooper minimum (or structural minimum) is deep and narrow (42, 45–47). Realization of controlling the line shape of a resonance as predicted in this work will be challenging but very interesting to prove the ease of controlling resonances at the few-ten attoseconds timescale. This work also indicates the significance of the temporal shape of attosecond XUV pulse, which has usually been ignored in most applications. Thus, it is desirable to identify its role under various scenarios of attosecond science.

Materials and Methods

For single-atom calculations, the three-level model of the helium atom has been established, which including the ground state $1s^2$, autoionizing states $2s2p$ and $2s^2$, and continuum states. With the aid of the Hamiltonian and TDSE, the coupled equation can be established and numerically solved by the Runge–Kutta method.

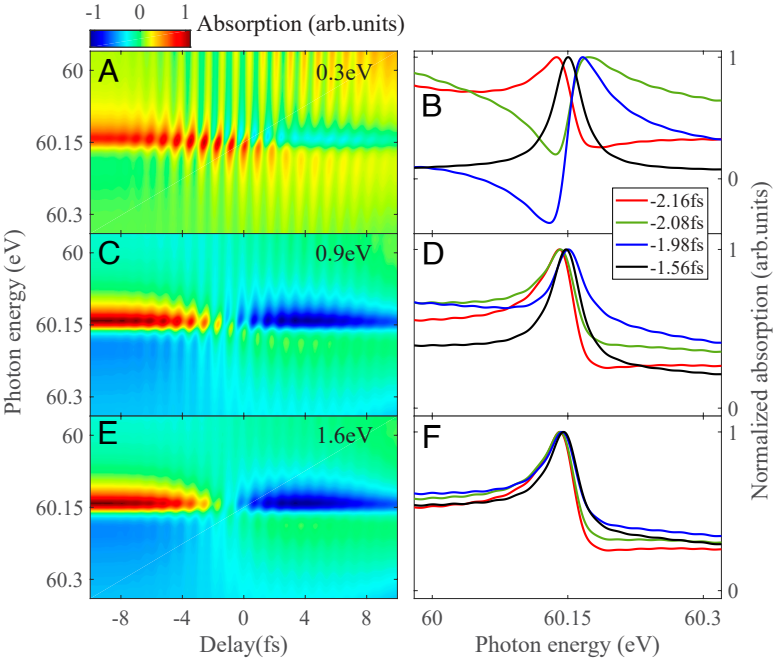

Fig. 5. ATA spectra when the minimum position of shaped XUV pulse is shifted by (*A* and *B*) 0.3 eV; (*C* and *D*) 0.9 eV; (*E* and *F*) 1.6 eV. Note that the oscillation with half optical period of IR laser can be clearly seen in (*A*), but not as obvious in (*C*) and (*E*).

For macroscopic propagation calculations, the one-dimensional Maxwell's wave equation in the moving frame has been adopted. The derivation of Eqs. **1**–**3** are based on coupled equations with some reasonable approximations. See *SI Appendix* for further details.

Data, Materials, and Software Availability. All study data are included in the article and/or *SI Appendix*.

ACKNOWLEDGMENTS. We acknowledge support from the National Natural Science Foundation of China under Grants Nos. 12274230, 12204238, and 11834004; Funding of Nanjing University of Science and Technology under Grant No. TSXK2022D005; Natural Science Foundation of Jiangsu Province under Grant No. BK20220925; and Chemical Science Division, Office of Basic Energy Sciences, Office of Science, US Department of Energy under Grant No. DE-FG02-86ER13491.

1. U. Fano, Effects of configuration interaction on intensities and phase shifts. *Phys. Rev.* **124**, 1866–1878 (1961).
2. S. Gilbertson *et al*., Monitoring and controlling the electron dynamics in helium with isolated attosecond pulses. *Phys. Rev. Lett.* **105**, 263003 (2010).
3. B. Yan, C. H. Greene, Coupled square well model and Fano-phase correspondence. *Phys. Rev. A* **95**, 032706 (2017).
4. C. L. M. Petersson, L. Argenti, F. Martín, Attosecond transient absorption spectroscopy of Helium above the N = 2 ionization threshold. *Phys. Rev. A* **96**, 013403 (2017).
5. M. Reduzzi *et al*., Observation of autoionization dynamics and sub-cycle quantum beating in electronic molecular wave packets. *J. Phys. B* **49**, 065102 (2016).
6. S. Beaulieu *et al*., Attosecond-resolved photoionization of chiral molecules. *Science* **358**, 1288–1294 (2018).
7. R. Y. Bello *et al*., Reconstruction of the time-dependent electronic wave packet arising from molecular autoionization. *Sci. Adv.* **4**, 3962 (2018).
8. S. Luo *et al*., Revealing molecular strong field autoionization dynamics. *Phys. Rev. Lett.* **126**, 103202 (2021).
9. K. Mizuyama, H. Cong Quang, T. Dieu Thuy, T. V. Nhan Hao, Classification of resonances and pairing effects on n–A scattering within the Hartree–Fock–Bogoliubov framework. *Phys. Rev. C* **104**, 034606 (2021).
10. K. Mizuyama, N. Le Nhu, T. V. Nhan Hao, Fano effect on neutron elastic scattering by open-shell nuclei. *Phys. Rev. C* **101**, 034601 (2020).
11. T. Fukuta, S. Garmon, K. Kanki, K. Noba, S. Tanaka, Fano absorption spectrum with the complex spectral analysis. *Phys. Rev. A* **96**, 052511 (2017).
12. D. Finkelstein-Shapiro, T. Pullerits, T. Hansen, Two-dimensional Fano lineshapes: Excited-state absorption contributions. *J. Chem. Phys.* **148**, 184201 (2018).
13. Z.-N. Farzad, R. Fleury, Topological Fano resonances. *Phys. Rev. Lett.* **122**, 014301 (2019).
14. M. Hentschel *et al*., Attosecond metrology. *Nature* **414**, 509–513 (2001).
15. P. M. Paul *et al*., Observation of a train of attosecond pulses from high harmonic generation. *Science* **292**, 1689–1692 (2001).
16. Z. X. Zhao, C. D. Lin, Theory of laser-assisted autoionization by attosecond light pulses. *Phys. Rev. A* **71**, 060702 (2005).
17. X. M. Tong, C. D. Lin, Double photoexcitation of He atoms by attosecond XUV pulses in the presence of intense few-cycle infrared lasers. *Phys. Rev. A* **71**, 033406 (2005).
18. T. Morishita, S. Watanabe, C. D. Lin, Attosecond light pulses for probing two-electron dynamics of helium in the time domain. *Phys. Rev. Lett.* **98**, 083003 (2007).
19. C. D. Lin, W.-C. Chu, Controlling atomic line shapes. *Science* **340**, 694–695 (2013).
20. W.-C. Chu, C. D. Lin, Theory of ultrafast autoionization dynamics of Fano resonances. *Phys. Rev. A* **82**, 053415 (2010).
21. W.-C. Chu, T. Morishita, C. D. Lin, Probing dipole-forbidden autoionizing states by isolated attosecond pulses. *Phys. Rev. A* **89**, 033427 (2014).
22. W.-C. Chu, S.-F. Zhao, C. D. Lin, Laser-assisted-autoionization dynamics of helium resonances with single attosecond pulses. *Phys. Rev. A* **84**, 033426 (2011).
23. W.-C. Chu, C. D. Lin, Absorption and emission of single attosecond light pulses in an autoionizing gaseous medium dressed by a time-delayed control field. *Phys. Rev. A* **87**, 013415 (2013).
24. W.-C. Chu, C. D. Lin, Photoabsorption of attosecond XUV light pulses by two strongly laser-coupled autoionizing states. *Phys. Rev. A* **85**, 013409 (2012).
25. X. Li *et al*., Investigation of coupling mechanisms in attosecond transient absorption of autoionizing states: Comparison of theory and experiment in xenon. *J. Phys. B.* **48**, 125601 (2015).
26. Z. Q. Yang, D. F. Ye, T. Ding, T. Pfeifer, L. B. Fu, Attosecond XUV absorption spectroscopy of doubly excited states in helium atoms dressed by a time-delayed femtosecond infrared laser. *Phys. Rev. A* **91**, 013414 (2015).
27. V. Gruson *et al*., Attosecond dynamics through a Fano resonance: Monitoring the birth of a photoelectron. *Science* **354**, 734–738 (2016).
28. A. Kaldun *et al*., Observing the ultrafast buildup of a Fano resonance in the time domain. *Science* **354**, 738–741 (2016).
29. L. Barreau *et al*., Disentangling spectral phases of interfering autoionizing states from attosecond interferometric measurements. *Phys. Rev. Lett.* **122**, 253203 (2019).
30. D. Busto *et al*., Time–frequency representation of autoionization dynamics in helium. *J. Phys. B* **51**, 044002 (2018).
31. M. Kotur *et al*., Spectral phase measurement of a Fano resonance using tunable attosecond pulses. *Nat. Commun.* **7**, 10566 (2016).
32. V. Stooß, M. Cavaletto, S. Donsa, A. Blättermann, P. Birk, Real-time reconstruction of the strong-field-driven dipole response. *Phys. Rev. Lett.* **121**, 173005 (2018).
33. L. V. Hau, S. E. Harris, Z. Dutton, C. H. Behroozi, Light speed reduction to 17 metres per second in an ultracold atomic gas. *Nature* **397**, 594–598 (1999).
34. N. S. Ginsberg, S. R. Garner, L. V. Hau, Coherent control of optical information with matter wave dynamics. *Nature* **445**, 623–626 (2007).
35. C. Ott *et al*., Strong-field extreme-ultraviolet dressing of atomic double excitation. *Phys. Rev. Lett.* **123**, 163201 (2019).
36. L. Aufleger *et al*., Pulse length effects on autoionizing states under the influence of intense SASE XUV fields. *J. Phys. B* **53**, 234002 (2020).
37. A. Magunia *et al*., Bound-state electron dynamics driven by near-resonantly detuned intense and ultrashort pulsed XUV fields. *Appl. Sci.* **10**, 6153 (2020).
38. G. Mouloudakis, P. Lambropoulos, Autoionizing states driven by stochastic electromagnetic fields. *J. Phys. B* **51**, 01LT01 (2018).
39. C. Ott *et al*., Lorentz meets Fano in spectral line shapes: A universal phase and its laser control. *Science* **340**, 716–720 (2013).
40. C. D. Lin, A.-T. Le, C. Jin, H. Wei, Elements of the quantitative rescattering theory. *J. Phys. B* **51**, 104001 (2018).
41. S. B. Schoun *et al*., Attosecond pulse shaping around a Cooper minimum. *Phys. Rev. Lett.* **112**, 153001 (2014).
42. C. Vozzi *et al*., Generalized molecular orbital tomography. *Nat. Phys.* **7**, 822 (2011).
43. A. Rupenyan, P. M. Kraus, J. Schneider, H. J. Wörner, Quantum interference and multielectron effects in high-harmonic spectra of polar molecules. *Phys. Rev. A* **87**, 013401(R) (2013).
44. A. Rupenyan, P. M. Kraus, J. Schneider, H. J. Wörner, High-harmonic spectroscopy of isoelectronic molecules: Wavelength scaling of electronic-structure and multielectron effects. *Phys. Rev. A* **87**, 033409 (2013).
45. C. Jin, S.-J. Wang, S.-F. Zhao, A.-T. Le, C. D. Lin, Robust control of the minima of high-order harmonics by fine-tuning the alignment of CO_2 molecules for shaping attosecond pulses and probing molecular alignment. *Phys. Rev. A* **102**, 013108 (2020).
46. C. Jin, S.-J. Wang, X. Zhao, S.-F. Zhao, C. D. Lin, Shaping attosecond pulses by controlling the minima in high-order harmonic generation through alignment of CO_2 molecules. *Phys. Rev. A* **101**, 013429 (2020).
47. H. J. Wörner, J. B. Bertrand, P. Hockett, P. B. Corkum, D. M. Villeneuve, Controlling the interference of multiple molecular orbitals in high-harmonic generation. *Phys. Rev. Lett.* **104**, 233904 (2010).
48. S. B. Zhang, X. T. Xie, J. G. Wang, Electron-spectral-line profiles of resonances by attosecond XUV or X-ray pulses. *Phys. Rev. A* **96**, 053420 (2017).
49. Y. He *et al*., Watching the formation and reshaping of a Fano resonance in a macroscopic medium. *Phys. Rev. A* **103**, L041102 (2021).
50. Z. Fu *et al*., Extension of the bright high-harmonic photon energy range via nonadiabatic critical phase matching. *Sci. Adv.* **8**, eadd7482 (2022).
51. H.-W. Sun *et al*., Extended phase matching of high harmonic generation by plasma-induced defocusing. *Optica* **4**, 976 (2017).
52. J. Pupeikis *et al*., Water window soft X-ray source enabled by a 25 W few-cycle 2.2 *mu*m OPCPA at 100 kHZ. *Optica* **7**, 168 (2020).
53. M. Krebs *et al*., Towards isolated attosecond pulses at megahertz repetition rates. *Nat. Photonics* **7**, 555–559 (2013).